INL/CON-08-14632
PREPRINT

Recent Progress at the Idaho National Laboratory in High Temperature Electrolysis for Hydrogen and Syngas Production

IMECE 2008

C. Stoots
J. O'Brien
J. Herring
J. Hartvigsen

November 2008

The INL is a
U.S. Department of Energy
National Laboratory
operated by
Battelle Energy Alliance

Proceedings of IMECE2008
2008 ASME International Mechanical Engineering Congress and Exposition
October 31 – November 6, 2008, Boston, USA

IMECE2008-68440

RECENT PROGRESS AT THE IDAHO NATIONAL LABORATORY IN HIGH TEMPERATURE ELECTROLYSIS FOR HYDROGEN AND SYNGAS PRODUCTION

C. STOOTS
Idaho National Laboratory
Idaho Falls, Idaho, USA
carl.stoots@inl.gov

J. O'BRIEN
Idaho National Laboratory
Idaho Falls, Idaho, USA
james.obrien@inl.gov

J. HERRING
Idaho National Laboratory
Idaho Falls, Idaho, USA
j.herring@inl.gov

J. HARTVIGSEN
Ceramatec, Inc.
Salt Lake City, Utah, USA
jjh@ceramatec.com

ABSTRACT

This paper presents the most recent results of experiments conducted at the Idaho National Laboratory (INL) studying electrolysis of steam and coelectrolysis of steam / carbon dioxide in solid-oxide electrolysis stacks. Single button cell tests as well as multi-cell stack testing have been conducted. Multi-cell stack testing used 10 x 10 cm cells (8 x 8 cm active area) supplied by Ceramatec, Inc (Salt Lake City, Utah, USA) and ranged from 10 cell short stacks to 240 cell modules. Tests were conducted either in a bench-scale test apparatus or in a newly developed 5 kW Integrated Laboratory Scale (ILS) test facility. Gas composition, operating voltage, and operating temperature were varied during testing. The tests were heavily instrumented, and outlet gas compositions were monitored with a gas chromatograph. The ILS facility is currently being expanded to 15 kW testing capacity (H_2 production rate based upon lower heating value).

INTRODUCTION

Crude oil prices have recently exceeded $140/barrel. Although part of the escalation in oil prices can be blamed on a weak dollar, ever-increasing worldwide demand for oil and worries over oil supply disruptions have also contributed to price increases. Predictions are that the price for crude oil in the long run will continue to increase. In spite of dramatic advances in oil exploration technologies, oil reserves discovered per exploratory well have dropped worldwide [1] and conventional world oil production will inevitably peak and no longer be able to keep up with demand. Many "peak oil" predictions claim that this will occur within the next 10 years.

Another problem with oil consumption has to do with carbon dioxide and global warming. A gallon of gasoline, when burned, produces almost 20 pounds of carbon dioxide. Another 5 pounds of carbon dioxide are produced per gallon during production and refining. 44% of the United State's energy related carbon dioxide emissions come from oil [2].

The combination of finite oil supply and global warming presents the world with a problem the magnitude of which it has never faced before. Previous energy transitions (wood to coal, coal to oil) were gradual. Oil peaking will likely be abrupt [1]. But, the fundamental problem with oil is that we do not have a substitute.

The United States is exploring the feasibility of a hydrogen-based energy economy, with the goals of reduced oil consumption, independence from foreign energy, and reduced greenhouse gas emissions. This hydrogen economy would rely upon water as a feedstock and non-carbon emitting energy sources (nuclear, wind, solar, etc.) to power the water splitting technology. For the past several years, the Idaho National Laboratory (INL), in conjunction with Ceramatec Inc. (Salt Lake City, Utah, USA) has had an on-going program funded by the Department of Energy (DOE) under the Nuclear Hydrogen Initiative (NHI) studying nuclear-powered high-temperature electrolysis of steam using solid-oxide cells for large-scale hydrogen production [3-6]. This program includes computational fluid mechanics modeling, systems process flowsheet studies, and experimental activities ranging from button cell testing (~1 W) and stack testing (~200 W) to multi-stack facility testing (~15 kW).

It is recognized, however, that the conversion to such a hydrogen-based energy economy will require decades. Synthetically-derived hydrocarbon fuels (synfuels) can offer a bridge to the future hydrogen economy and an interim solution to obtain domestic energy independence. The raw material for synfuel production is syngas, a mixture of hydrogen (H_2) and carbon monoxide (CO). Traditionally, syngas has been produced via coal gasification, and more recently by steam reforming of natural gas. Both techniques consume non-renewables and emit greenhouse gases.

The INL in collaboration with Ceramatec Inc. has also been studying the extension of high temperature solid-oxide based steam electrolysis to the coelectrolysis of steam and carbon dioxide to produce syngas:

$$H_2O + CO_2 \xrightarrow{electricity,heat} \underbrace{H_2 + CO}_{syngas} + O_2 . \quad (1)$$

Coelectrolysis is a significantly more complicated process than steam electrolysis, and is not completely understood. It has not been shown conclusively that coelectrolysis of steam and CO_2 actually proceeds by electrolysis of both CO_2 and H_2O, or whether steam is electrolyzed predominantly or even exclusively to produce hydrogen that immediately reacts with CO_2 to produce CO via the reverse shift reaction (RSR):

$$CO_2 + H_2 \leftrightarrow CO + H_2O. \quad (2)$$

The thermodynamic reversible voltage or Nernst potential of the CO-CO_2 and H_2-H_2O electrolysis/fuel cell reactions are identical if the shift reaction is at equilibrium, so thermodynamic potential does not favour one reaction pathway over the other. However, one might expect the lighter and smaller molecules of the H_2-H_2O pair to have faster kinetics than the much heavier CO-CO_2 molecules. Fuel cell testing at Ceramatec in the early 1990's showed that the area specific resistance (ASR) of SOFC button cells operating on a dry CO-CO_2 feed was a factor of 10 greater than for the same cell operating with humidified hydrogen (i.e. H_2-H_2O). Although the I-V sweep with dry CO-CO_2 was not extended above the open circuit voltage into the electrolysis regime at the time, experience has shown virtually identical cell performance in fuel cell and electrolysis modes. That is, given sufficient availability of reactants for both fuel cell and electrolysis operation, the I-V curve is linear from electrolysis mode, through open circuit and into fuel cell mode.

Electrode materials and structure development over the past 15 years at Ceramatec have closed the performance gap such that cell ASR is now only about 50% greater for dry carbon dioxide electrolysis than steam electrolysis. This result has been shown in single cell testing at Ceramatec, and in 10 cm cell stack testing at INL. However, with the introduction of even a small amount of steam or hydrogen to a predominantly CO-CO_2 reactant stream, the cell performance is virtually identical to that of the cell on H_2-H_2O alone (see Figure 5 below). This is true even when the flow rates of H_2-H_2O are insufficient to support the cell current. Either CO-CO_2 is utilized by the shift reaction, with H_2-H_2O participating in the electrochemical reaction, or the presence of H_2-H_2O catalyzes the electrochemical reactions of CO-CO_2 by formation of some surface intermediate. Regardless of the mechanism, the practical implication is that coelectrolysis is preferred to dry electrolysis of CO_2. An even more important reason that dry CO_2 electrolysis is not recommended is because under most conditions the reduction potential of CO to solid carbon is only slightly higher than for CO_2 to CO. Under conditions of high CO_2 conversion, the reduction potential of CO actually becomes less than that of CO_2 making carbon deposition difficult to avoid. In coelectrolysis, CO concentrations are decreased by the presence of steam and hydrogen, such that carbon deposition by electrochemical reduction of CO is not generally possible.

Some results of steam electrolysis and coelectrolysis experiments performed to date using button cells, stacks, and the ILS facility are presented and discussed. These results include electrolysis performance at various temperatures, gas mixtures, and electrical settings. For coelectrolysis, product gas compositions as measured via an online micro gas chromatograph (GC) are compared to predictions obtained from an INL-developed chemical equilibrium coelectrolysis model (CECM). An inline methanation reactor has also been tested to study direct methane production from coelectrolysis products. When linked to nuclear power, high temperature electrolysis can offer a carbon-free means for large scale H_2 production while coelectrolysis can provide a carbon neutral means of producing syngas while consuming CO_2.

CURRENT EXPERIMENTAL TESTING FACILITY

A comprehensive discussion of the INL high temperature solid oxide electrolysis bench scale experiment is presented elsewhere [3, 4, 6, 7]. This same facility is used for button cell testing as well as stack testing. A photograph of the test hardware is found in Figure 1. Primary components include gas supply cylinders, mass-flow controllers, a humidifier, dewpoint measurements stations, microchannel gas chromatograph, temperature and pressure measurement, high temperature furnaces, and a solid oxide electrolysis cell/stack.

For single-cell testing, an electrolysis button cell is bonded to the bottom of a zirconia tube, as shown in Figure 2. During testing, the tube is suspended in the smaller furnace. The cell is an electrolyte-supported single button cell with a scandia-stabilized zirconia electrolyte, about 150 μm thick. The outside electrode, which acts as the cathode in fuel cell mode and the anode in electrolysis mode, is a doped manganite. The inside electrode (electrolysis cathode) material is a nickel cermet. Both button-cell electrodes incorporate a platinum wire mesh for current distribution. The button cell includes both an active cell area (2.5 cm^2 for the cell shown) and a reference cell area. A type-K stainless-steel sheathed thermocouple is mounted on the manifold tube and bent around in front of the button cell in

Fig. 1. Photograph of the INL high-temperature electrolysis laboratory.

order to allow for continuous monitoring of the button-cell temperature.

For stack testing, the inlet gas mixture is directed to the larger high temperature furnace, which heats and maintains the electrolyzer at the appropriate test temperature via computer-based feedback control. The furnace also preheats the inlet gas mixture and the air sweep gas. A photograph of the stack, mounted on its inconel test fixture and resting on the furnace base, is shown in Figure 3. The button cells and stacks were fabricated by Ceramatec, Inc., of Salt Lake City, UT. The stacks have a per-cell active area of 64 cm^2, for a total active area of 640 cm^2 each.

The piping and instrumentation schematic for the ILS single-module experiment with no heat recuperation or hydrogen recycle is shown in Figure 4. The ILS facility is currently being expanded to accommodate three modules as well as heat recuperation and hydrogen recycle. The electrolysis module requires a support system supplying electrical power for electrolysis, a feedstock gas mixture of hydrogen and steam, a sweep gas, and appropriate exhaust handling. In particular, this system must include means for

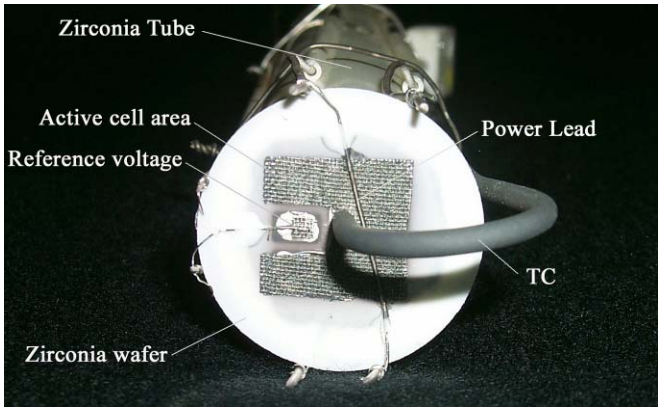

Fig. 2. Detail of button cell.

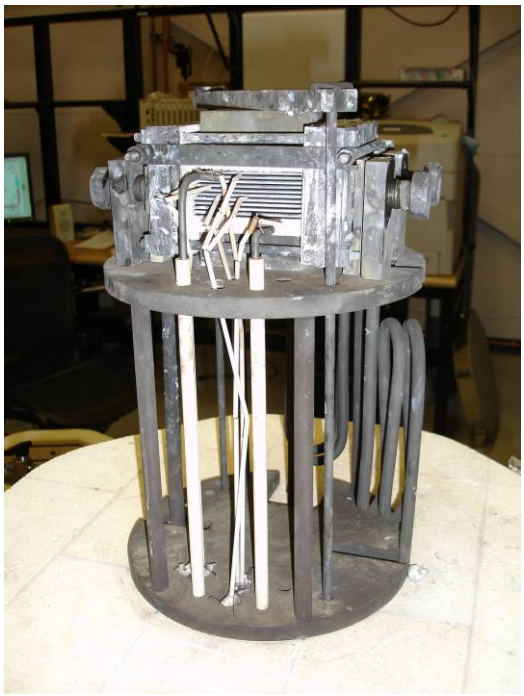

Fig. 3. 10-cell stack mounted on test fixture on furnace base, ready to test.

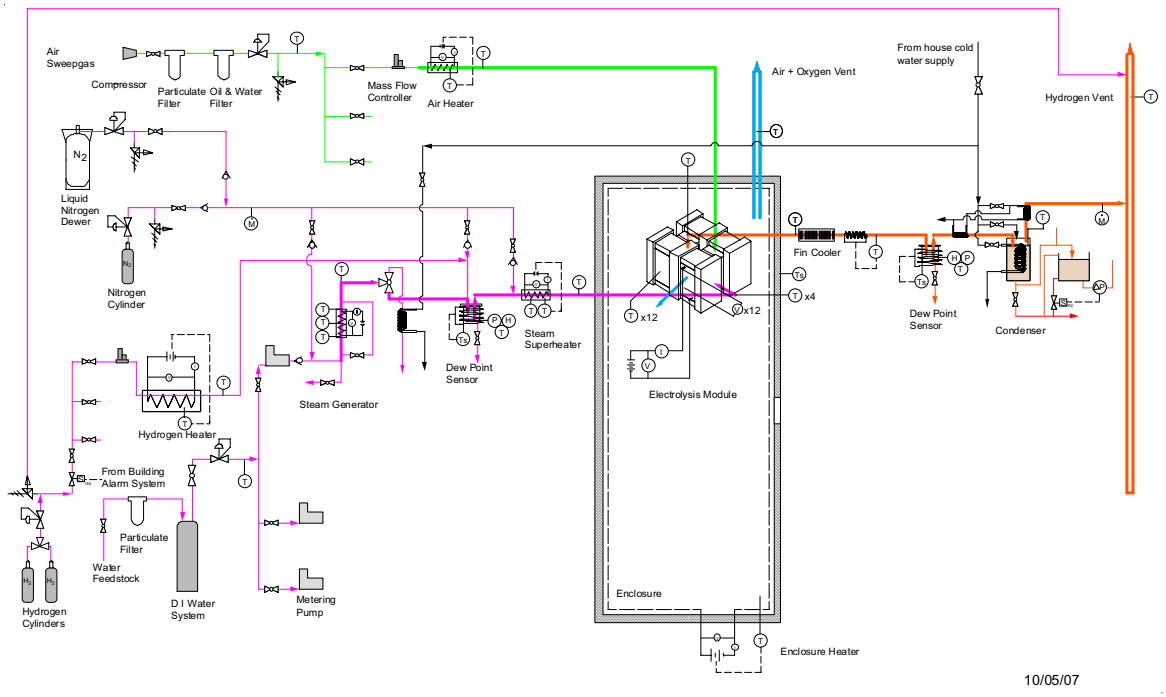

Fig. 4. ILS single module piping and instrumentation schematic.

controlled steam generation, mixing hydrogen with the steam, feedstock and product dewpoint measurements, heating the feedstock and sweep gas to the appropriate electrolysis temperature (via a superheater), cooling the electrolysis product stream, condensing any residual steam out of the product stream, and venting the hydrogen product. The final ILS support system will consist of three parallel systems that supply feedstock, sweep gas streams, and electrical power basically independent of each other to each of three modules. All three modules will be located within a single hot zone. The facility is designed to accommodate later incorporation of heat recuperation and hydrogen recycle capabilities. To aid in interpretation of Figure 4, the hydrogen / steam feedstock is represented by the color magenta, the product stream by orange, the inlet sweep gas by green, and the outlet sweep gas by blue.

Fig. 5. Hot zone enclosure with one module installed.

Liquid water feedstock is fed at a controlled rate into the system by means of a positive-displacement metering pump. The water is then vaporized and slightly superheated in an inline electrically-powered steam generator. The steam generator was fabricated by attaching a combination of fifteen 200 and 300 watt clamp-on electric heaters to the outside of a 1" diameter stainless steel tube. The heaters are covered with 2" of thermal insulation, then topped by an aluminum covering. The heaters are spaced such that a higher heat flux is obtained in the boiling region and lower heat flux in the single-phase regions. The heaters are all wired in parallel so that each operates at the same voltage. The tube interior is filled with a copper foam material which reduces flow perturbations and increases temperature uniformity in the boiling region. The outlet temperature is controlled by carefully adjusting the input power supplied by a DC power supply to obtain the desired superheat temperature.

The slightly superheated steam exiting the steam generator is mixed with hydrogen, which is required on the inlet side of the stack in order to maintain reducing conditions at the steam/hydrogen electrode. In the initial ILS configuration (prior to the implementation of hydrogen recycle), the inlet hydrogen will be supplied from a compressed gas bottle. The hydrogen flow rate is controlled by a mass-flow controller and the data acquisition / control system (DACS). The inlet hydrogen must be heated to the steam generator outlet temperature in order to prevent cooling of the steam and

Fig. 6. INL ILS facility, with major components labeled.

possible steam condensation. This is accomplished by temperature-based feedback control of the hydrogen preheater powered by a DC power supply in conjunction with the DACS.

TABLE I
Component identifiers for Figure 6.

ID	Component
1	Electrolysis stacks / module
2	Hot zone enclosure lid
3	Power supply and instrument racks
4	Electrical distribution cabinets
5	Data acquisition and control monitors
6	Deionized water system
7	Water supply metering pump
8	Steam generator
9	H_2 preheater
10	Steam and H_2 superheater
11	Air compressor
12	Air heater
13	Product finned cooler
14	Steam condenser
15	Condensate tank
16	H_2 mass flow meter
17	H_2 vent
18	Air and O_2 vent
19	Dew point sensor

Downstream of the mixing point, the temperature, pressure, and dewpoint of the steam/hydrogen gas mixture are measured. The absolute pressure is directly measured at the dewpoint measurement station in order to allow for accurate determination of the steam mole fraction. Precise measurement of the dewpoint and pressure allows for independent determination of the inlet gas composition.

A high-temperature electrically powered inline superheater then boosts the feedstock stream to the final electrolyzer operating temperature, 800° - 830°C. Heat is supplied from six semi-cylindrical ceramic-fiber heaters with embedded coiled elements. Each heater section is capable of providing 1800 watts of power when operated at 240 volts, but they are operated at a much lower voltage for this application. Power is supplied to the heaters from 3.3 kW DC power supplies. Heater power is feedback-controlled based on thermocouples located inside the ceramic fiber heaters. Two inch thick high-temperature thermal insulation is wrapped around the heaters and covered with an aluminum skin.

The primary material of construction for the low-temperature tubing and components upstream of the superheater is 316 stainless steel. For high temperatures such as 800°C, Inconel 600 tubing is used within the superheater and air heater.

The electrolysis module is mounted in the hot zone enclosure (Figure 5) where it is maintained at the desired operating temperature using radiant heaters installed in the sides and top of the removable lid. As explained in reference

[8], when the electrolysis process is operated below the thermal neutral voltage (voltage at which stack ohmic heating balances the endothermic heat requirement, V_{tn} = 1.287 V/cell for 800°C operating temperature), heat must be added to overcome the endothermic reaction heat requirement. At thermal neutral conditions, the module operation is adiabatic and isothermal. If, however, the module is operated above the thermal neutral voltage, heat must be removed from the system.

The base of the hot zone enclosure consists of a stainless steel plate covered with several inches of high-temperature insulation, as shown in Figure 5. The module rests on top of the insulation. The process streams, power leads, and instrumentation access the module through holes in the bottom plate and insulation. A stainless-steel lid covers the hot zone enclosure and is sealed against the bottom plate with an O-ring. The radiant heater panels are powered by a DC power supply, feedback-controlled based on a thermocouple mounted inside the enclosure. The lid is attached to screw-drive rods on each end, driven by an electric motor, which allow for convenient raising and lowering of the lid.

The gas mixture exiting the electrolyzer will be significantly enriched in hydrogen, typically to at least 50% hydrogen mole fraction, with the remainder being residual steam. The product stream is first cooled via a natural-convection air-cooled heat exchanger. The product stream temperature exiting this cooler is controlled such that no condensation can occur. Then the product gas mixture enters the outlet dewpoint measurement station. As discussed previously, the measurement of both inlet and outlet dewpoint temperatures allows for direct determination of the steam consumption rate, and the corresponding hydrogen production rate. This rate can be compared to the electrochemical hydrogen production rate determined from the stack electrical current. The outlet hydrogen/steam flow then enters a condenser where the vast majority of the residual steam is removed. The rate of water condensation is monitored via tank level, providing an additional independent measure of steam consumption. At this point, the product stream will be ambient-temperature, saturated hydrogen gas, with about 2.7% residual water vapor. The flow rate of this product gas is measured with a low-pressure-drop mass flow transducer. Comparison of the condensate and hydrogen product mass flow rates with the electrolyzer inlet mass flow rates helps quantify any stack leakage that may occur. The hydrogen product is then vented from the building.

Air is used as a sweep gas to remove excess oxygen from the ILS system. Filtered compressed air flows through a mass-flow controller and into an electrically-powered heater to preheat the inlet air to the stack operating temperature. Downstream of the electrolyzer, the hot oxygen-enriched air stream is then vented from the building to the environment.

Nitrogen gas can be injected directly into the steam superheater. This feature is used during startup until the superheater outlet temperature reaches about 400ºC to preclude any liquid entering the electrolysis module. During some scenarios, nitrogen gas may continue to be injected during steady state operation. For instance, if a module is found to be particularly leaky, nitrogen can be used to increase the average molecular weight of the gas mixture and hence reduce hydrogen diffusion rates. The nitrogen can be supplied from either a compressed gas cylinder or from a liquid nitrogen Dewar.

Detailed process flow sheets were developed for the ILS design using the commercial system-analysis code UniSim. These flow sheets include all of the components present in the actual ILS facility such as pumps, heaters, condensers, and the electrolyzer. Since the electrolyzer is not a standard UniSim component, a custom one-dimensional electrolyzer model was developed for incorporation into the overall process flow sheet. This electrolyzer model allows for the determination of the H_2 production rate, average Nernst potential, cell operating voltage, gas outlet temperatures, and electrolyzer efficiency for any specified inlet steam, hydrogen, and sweep-gas flow rates, current density, cell active area, and external heat loss or gain. The model includes a temperature-dependent area-specific resistance (ASR) that accounts for the significant increase in electrolyte ionic conductivity that occurs with increasing temperature. Details concerning this one-dimensional model and its implementation in UniSim have been reported in [8, 9].

All of the system components and hardware were mounted on a skid that is 16 ft. long by 10 ft wide. A photograph of the ILS skid with the components identified is presented in Figure 6. The components are listed in Table I by identification number. A custom LabView (National Instruments) program was developed for ILS data acquisition and instrument control using SCXI data acquisition hardware.

ELECTROLYSIS STACKS AND MODULES

Planar stacks used for testing by the INL are fabricated by Ceramatec, Inc., of Salt Lake City, UT. The internal components of the stack are shown in Figure 7 and are comprised as follows. The interconnect plate is fabricated primarily from ferritic stainless steel. It includes an

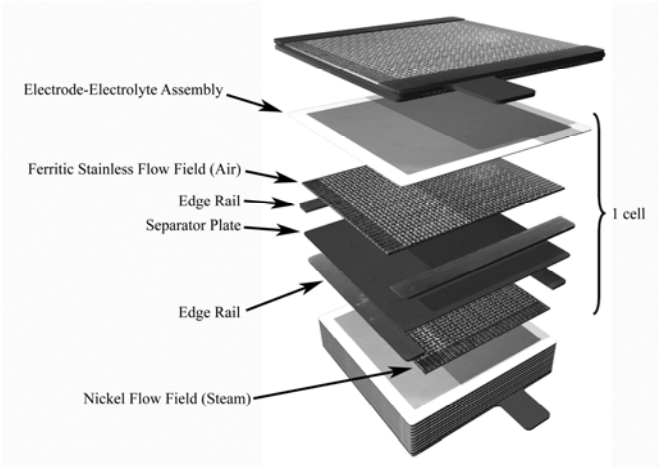

Fig. 7. Diagram of solid-oxide stack components.

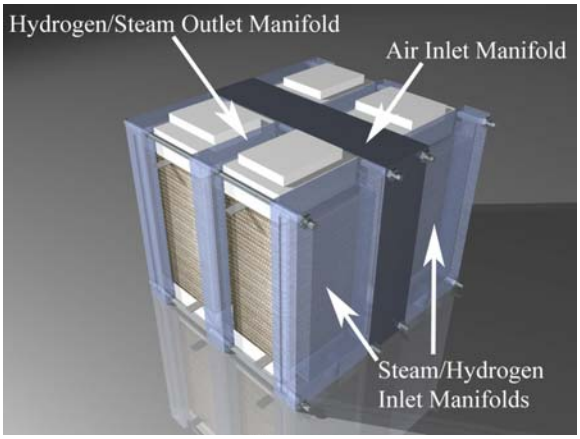

Fig. 8. ILS 4-stack module.

impermeable separator plate (~0.46 mm thick) with edge rails and two corrugated flow fields, one on the sweep-gas side and one on the steam / hydrogen side. The height of the flow fields is 1.0 mm. Each flow field includes 32 perforated flow channels across its width to provide uniform gas-flow distribution. The steam / hydrogen flow fields are fabricated from nickel foil. The air-sweep flow fields are made from ferritic stainless steel. The interconnect plates and flow fields also serve as electrical conductors and current distributors. To improve performance, the sweep-side separator plates and flow fields are surface-treated to form a rare-earth stable conductive oxide scale. A perovskite rare-earth coating is also applied to the separator plate oxide scale by either screen printing or plasma spraying. On the steam / hydrogen side of the separator plate, a thin (~10 μm) nickel metal coating is applied.

The electrolyte is scandia-stabilized zirconia, ~140 μm thick. The sweep-side electrode (anode in the electrolysis mode) is a strontium-doped manganite. The electrode is graded, with an inner layer of manganite/zirconia (~13 μm) immediately adjacent to the electrolyte, a middle layer of manganite (~18 μm), and an outer bond layer of cobaltite. The steam / hydrogen electrode (cathode in the electrolysis mode) is also graded, with a nickel cermet layer (~13 μm) immediately adjacent to the electrolyte and a pure nickel outer layer (~10 μm).

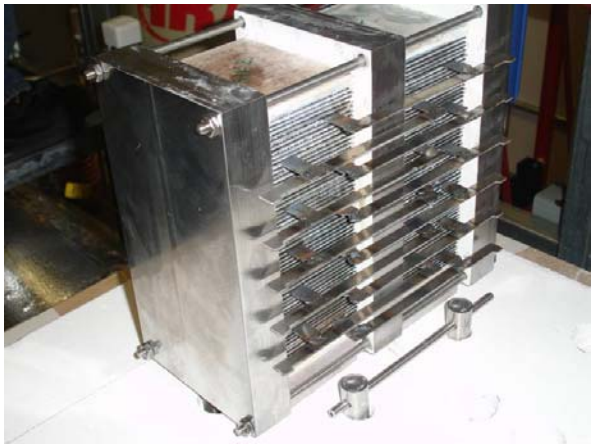

Fig. 9. One-half of ILS module showing electrical interconnections.

Fig. 10. ILS module with spring-loaded compression bars.

In the INL ILS facility, four sixty-cell stacks are combined into a module (see Figure 8). Each cell has an active area of 64 cm^2 per cell, providing a total active area of 15,360 cm^2 in a module. They are designed to operate in cross flow, with the steam / hydrogen gas mixture entering the inlet manifolds on the right and left sides, and exiting through the outlet manifold visible in Figure 8. Airflow enters through an air inlet manifold (Figure 8) and exits through the front and back open faces directly into the hot zone enclosure.

Each pair of stacks is called a half module (Figure 9). To preclude the loss of an entire stack if a single cell fails, the four stacks are electrically interconnected at every fifth cell. This is done by first electrically interconnecting the pair of stacks in

TABLE II.

ILS single module design parameters.

Independent Design and Operational Parameters	
active cell area	64 cm^2
cells per stack	60
number of stacks	4
stack operating temperature	830°C
steam utilization	50%
stack operating voltage	77 V
per-cell ASR	1.5 Ωcm^2
inlet steam mole fraction	0.9
inlet hydrogen mole fraction	0.1
Anticipated Performance Values	
per-cell operating voltage	1.283 V
current density	0.25 A/cm^2
stack power	1232 W
total power (electric)	4.85 kW
inlet hydrogen flow rate	5.8 NLPM
inlet steam flow rate	53 NLPM
inlet liquid water flow rate	0.7 g/s
air flow rate	22.6 NLPM
hydrogen production rate	1578 NL/hr
heating value of hydrogen produced	4.7 kW (LHV)

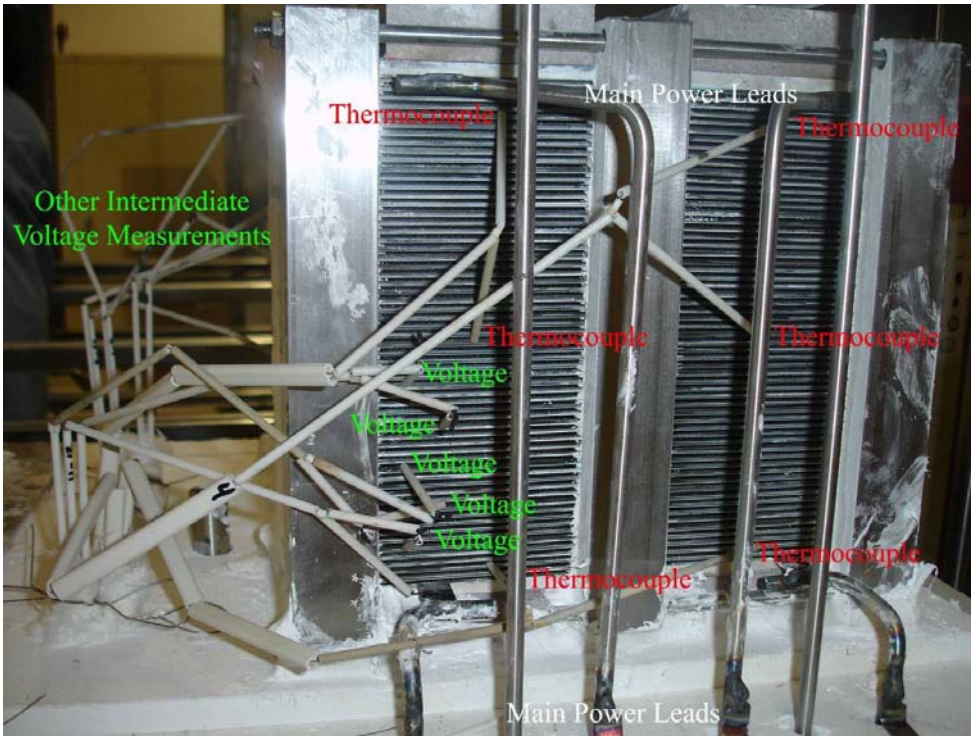

Fig. 11. Final installation of ILS module with instrumentation and power attachments.

each half module (Figure 9), and then interconnecting the two half modules when they are in final position. When the two half-modules are placed back-to-back a common air inlet plenum for all four stacks is formed. Spring loaded bars are placed over the stacks to maintain a compressive load on the stacks during operation (Figure 10). Power leads to each stack, intermediate voltage taps and interior thermocouples were then attached, and subsequent sealing of gaps completed the installation (Figure 11).

A summary of the operating parameters and nominal predicted performance characteristics of the ILS for one module is provided in Table II. Three modules will be incorporated in the final ILS configuration, each of which will include 4 stack sof 60 cells each, totaling 720 cells. The nominal performance of the 3-module system can be scaled from Table II.

SAMPLE BUTTON CELL TEST RESULTS

Open-cell potentials are monitored continuously during heatup as a system diagnostic. A significant departure of measured open-cell potentials from predicted values can indicate a problem such as a cracked cell or a short circuit. A plot of open-cell potentials measured during heatup with both the active cell (V_{op}) and the reference cell (V_{ref}) is presented in Figure 12. The gas flow rates and inlet dewpoint values used during the heatup are indicated in the figure. Predicted Nernst potentials based on temperature-dependent equilibrium compositions:

$$V_N = \frac{-\Delta G_{f,H_2O}(T)}{2F} - \frac{R_u T}{2F}\ln\left[\left(\frac{y_{1,H2O}}{y_{1,H2}y_{O2}^{1/2}}\right)\left(\frac{P}{P_{std}}\right)^{-1/2}\right] = \frac{-\Delta G_{f,CO_2}(T)}{2F} - \frac{R_u T}{2F}\ln\left[\left(\frac{y_{1,CO2}}{y_{1,CO}y_{O2}^{1/2}}\right)\left(\frac{P}{P_{std}}\right)^{-1/2}\right] \quad (3)$$

are also shown. In Equation 3, y represents component mole fraction, R_u is the ideal gas constant, F is the Faraday constant, ΔG is the Gibbs free energy of formation, P is the experimental operating pressure, and P_{std} is standard pressure, T is the

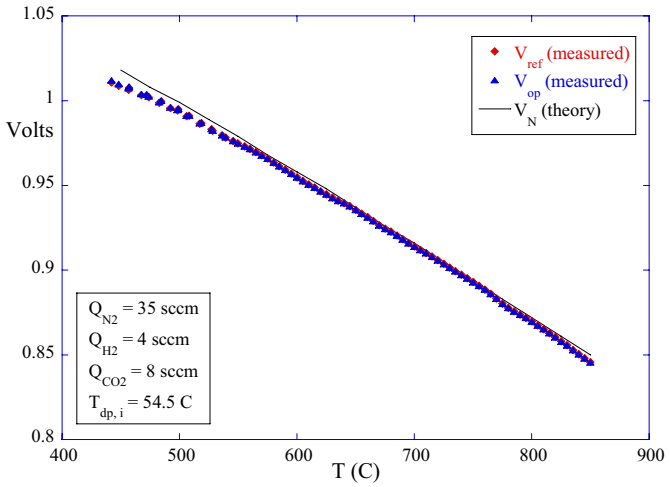

Fig. 12. Open-cell potential during heatup, measured and. predicted.

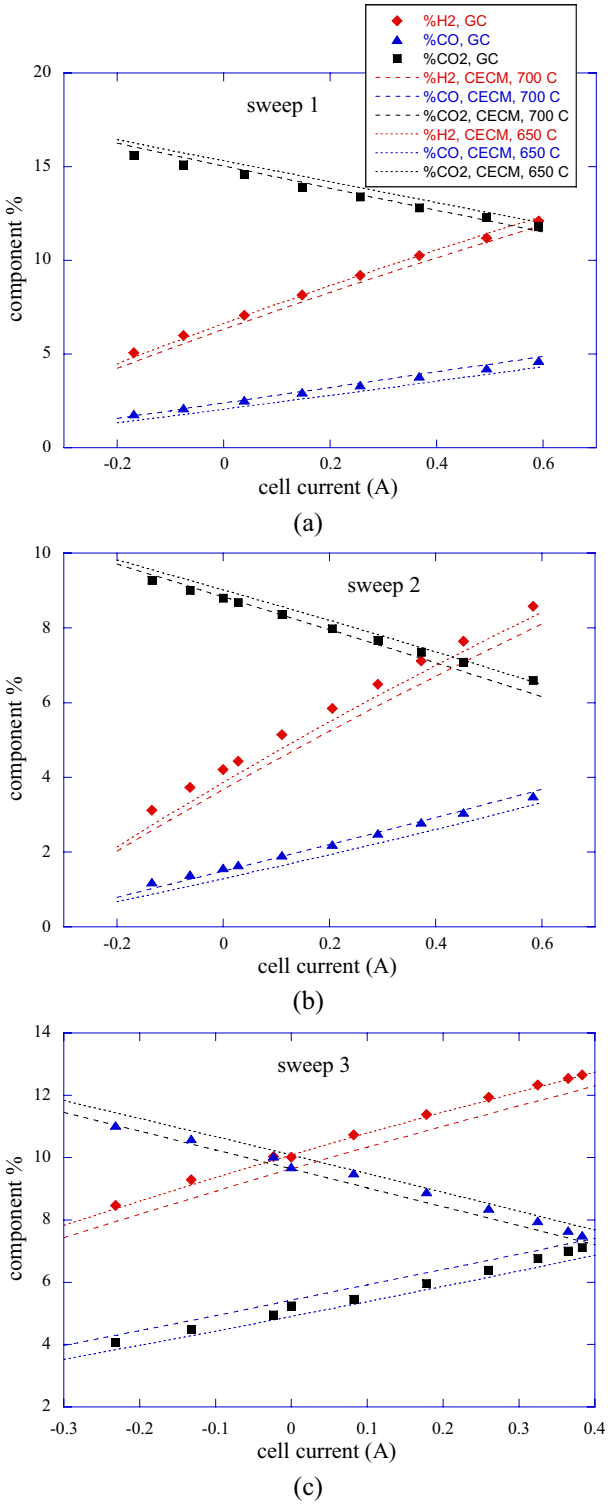

Fig. 13. Measured outlet gas compositions, with comparisons to predictions from the chemical equilibrium coelectrolysis model, sweeps 1 – 3.

experimental operating temperature. Above 500°C, agreement between the measured potentials and theoretical values is generally within a few millivolts.

Coelectrolysis performance was characterized through a series of stepwise DC potential sweeps. Results of three sweeps are presented in Figures 13(a-c). The furnace temperature for all three sweeps was 800°C. The flow rates used for these test were quite small. Low flow rates were required in order to achieve reasonable steam and CO_2 utilization values with low values of total cell current. The single cell, with an active area of 2.5 cm^2, could only support a maximum total current of about 0.75 A.

The effect of electrolysis on gas composition is shown in Figures 13(a – c). These figures plot the mole percent of H_2, CO, and CO_2 as a function of cell current, on a dry basis, for the same three sweeps plotted in Figure 13. The data symbols represent measurements obtained from the gas chromatograph. The lines represent predictions based upon a INL-developed chemical equilibrium coelectrolysis model (CECM). Two lines are shown for each case. The dashed lines represent CECM predictions based on an effective equilibrium temperature of 700°C. The dotted lines represent CECM predictions based on an effective equilibrium temperature of 650°C.

During coelectrolysis, the mole fractions of CO_2 and steam (not shown in Fig. 13) decrease with current, while the mole fractions of H_2 and CO increase. For the conditions chosen for these tests, the ratio of H_2 to CO is close to the desired 2-to-1 value for syngas production. Measured compositions of CO_2 and CO agree best with predictions based on an effective equilibrium temperature of 700°C. Measured compositions of H_2 agree best with predictions based on an effective equilibrium temperature of 650°C.

SAMPLE STACK TEST RESULTS

Within the past year, two 10-cell stacks were tested at the INL under steam and coelectrolysis conditions. Both stacks were heated under identical initial conditions: 3000 sccm N_2 flow rate, 497 sccm H_2 flow rate, and an inlet gas dew point temperature of 51.8 C. However, in the case of stack #2, once

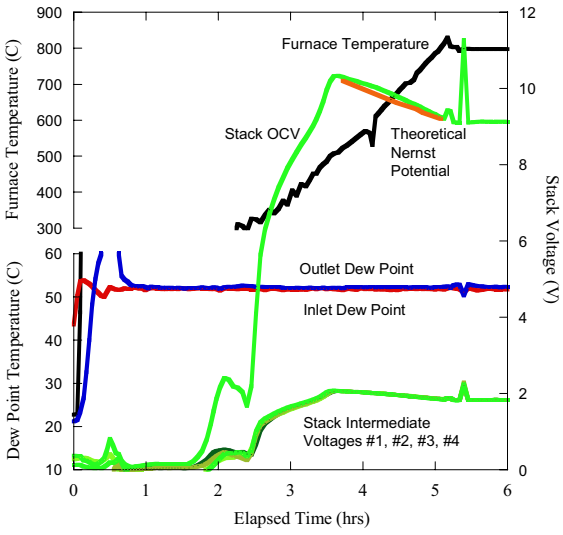

Fig. 14. Heat-up results for stack #1.

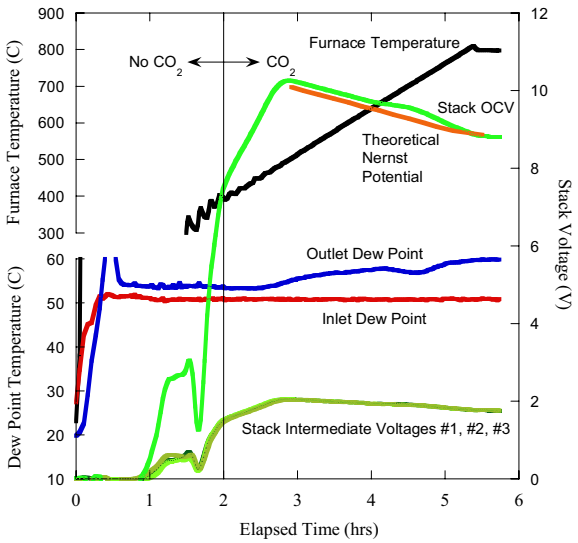

Fig. 15. Heat-up results for stack #2.

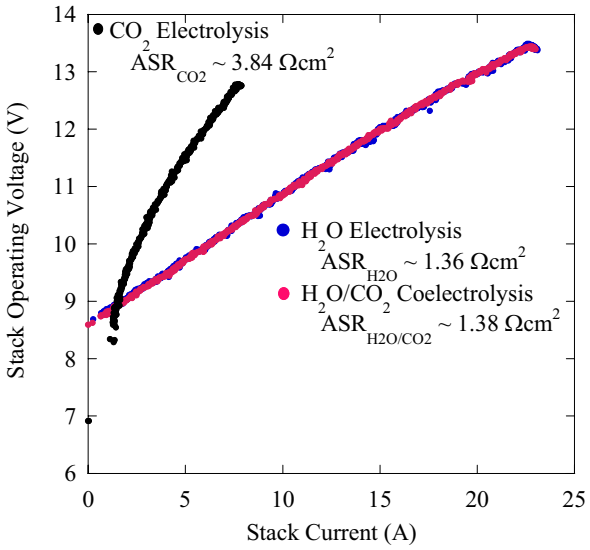

Fig. 16. Polarization curves for H_2O electrolysis, H_2O/CO_2 coelectrolysis versus CO_2 coelectrolysis, with mean ASR values.

all internal stack temperatures were above 350 C (or, after about 2 hours of heat up), 750 sccm of CO_2 was also introduced. Figures 14 and 15 show the heat-up profiles for stacks #1 and #2, respectively. Both stacks demonstrated remarkably similar heat-up profiles. The stacks do not exhibit an open cell potential (OCV) until above approximately 300-350 C, at which point the electrolyte begins to become an ion conductor. The orange lines represent the theoretical Nernst potentials for the gas mixtures, agreeing quite well with the measured OCVs. Of interest is that in the case of stack #2, the outlet dew point temperature begins to climb as the furnace temperature exceeds 450 C, indicating that the RSR has begun to reduce CO_2 and produce H_2O.

Cell ASR is dependent upon the type of electrolysis being conducted, with pure CO_2 electrolysis exhibiting a significantly higher ASR than steam electrolysis. However, in coelectrolysis the RSR is probably relied upon for most CO_2-to-CO conversion, and steam electrolysis is the primary electrolytic reaction. Therefore, there is little change in ASR from steam electrolysis to coelectrolysis. To demonstrate this, polarization curves were generated for stack #3 for steam electrolysis, H_2O/CO_2 coelectrolysis, and CO_2 electrolysis. Once the stack was at the operating temperature of 800°C, a steam electrolysis polarization curve was generated by performing a voltage sweep for the conditions T = 800°C, H_2 = 996 sccm, CO_2 = 0 sccm, N_2 = 1009 sccm, with 54.8 mol% H_2O inlet. This same voltage sweep was repeated for coelectrolysis conditions T = 800°C, H_2 = 996 sccm, CO_2 = 1003 sccm, N_2 = 0 sccm, with 54.9 mol% H_2O inlet and for CO_2 electrolysis conditions T = 800°C, H_2 = 0 sccm, CO_2 = 1500 sccm, N_2 = 0 sccm, with 0 mol% H_2O inlet. These results are shown in Figure 16.

There was almost no change in apparent ASR for coelectrolysis versus steam electrolysis. However, the ASR for CO_2 electrolysis was significantly higher, reinforcing the hypothesis that steam electrolysis is the principal electrolysis reaction and that the RSR is mostly responsible for CO production.

Typical results of coelectrolysis sweep composition measurements are presented in Figure 17. This figure presents the compositions of steam, CO_2, hydrogen, and CO as a function of electrolysis current on a dry basis for stack #1. Conditions for this test were T = 800°C, H_2 = 497 sccm, CO_2 = 505 sccm, N_2 = 2510 sccm, with 11.4 mol% H_2O inlet. Lines represent various model predictions and symbols represent experimental measurements. Figure 17 shows that even at zero current there was a drop in CO_2 and H_2 mole fractions from the cold inlet values, with CO produced. This is solely due to the RSR. As the electrolysis current was increased, the yield of

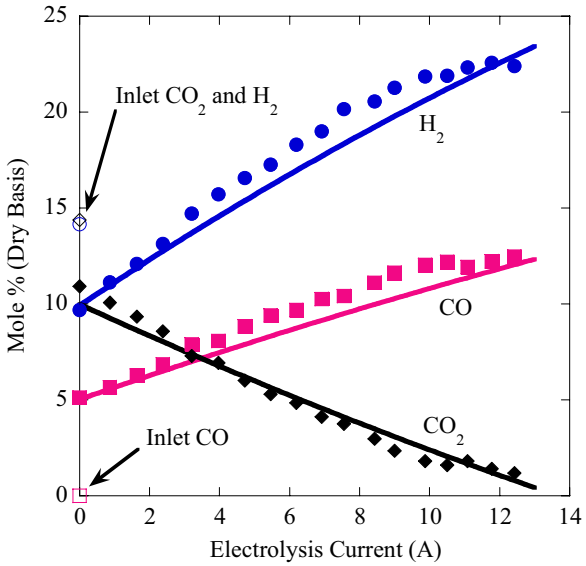

Fig. 17. Test 3 experimental and chemical equilibrium coelectrolysis model results, T_{equil} = 800 C.

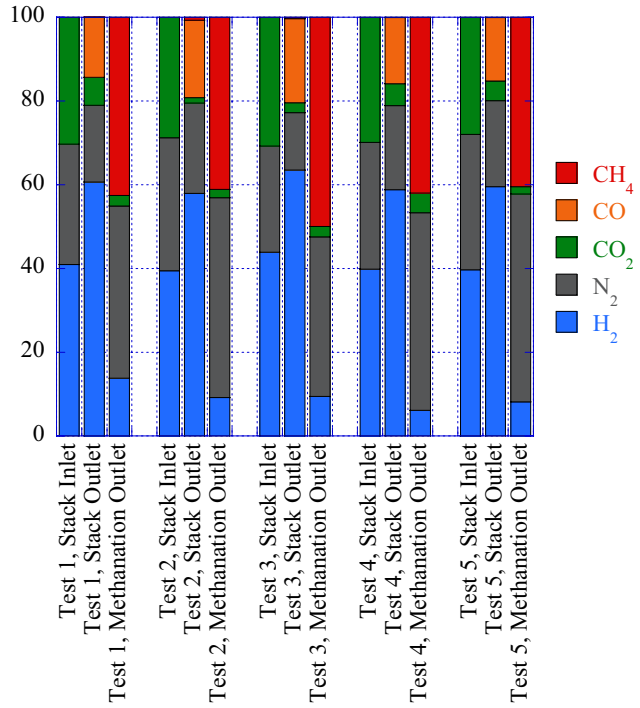

Fig 18. Coelectrolysis with subsequent methanation.

syngas increased linearly while the concentration of CO_2 (and H_2O, not shown in the figures) decreased. Results also show overall good agreement between experimental GC data and results from the chemical equilibrium coelectrolysis model for the range of testing performed in this study.

Ceramatec Inc. extended their 10-cell stack testing apparatus by addition of a methanation reactor downstream of the stack. The methanation reactor consisted of a 18 mm inner diameter stainless steel tube, approximately 1.5 m in length. Within this tube was placed a commercial steam reforming catalyst (R-67R from Haldor Topsoe). This is a nickel catalyst on magnesium aluminate, a ceramic inert oxide of the spinel family. The reactor tube was placed within a zinc-aluminum sleeve to homogenize the axial temperature gradient. The reactor was maintained at approximately 300 C for testing. Testing consisted of high temperature coelectrolysis, with the coelectrolysis products immediately fed to the methanation reactor. Figure 18 summarizes the stack inlet, stack outlet, and methanation outlet stream compositions (volume %) for 5 tests. Between 40 and 50 volume % methane product was produced.

SAMPLE ILS TEST RESULTS

The INL ILS facility was first operated in the summer of 2007 with one 240 cell module in place. After heatup of the module, the facility was set at the operating conditions listed in Table III. The ILS module performance was tested by sweeping the module power supply voltage over the range of 50 to 79 V (0.83 V/cell to 1.32 V/cell). This range corresponds to operation from the open-cell voltage to slightly above the thermal neutral voltage. The operating conditions for the ILS

TABLE III.

Operating conditions for ILS module voltage sweep.

Hot zone temperature	820 C
Inlet water mass flow rate	34 ml/min
Inlet H_2 flow rate	5.4 Nl/min
Inlet N_2 flow rate	5.4 Nl/min
Inlet Air flow rate	25 Nl/min
Predicted OCV	50.5 V
Measured OCV	49.6 V
Predicted inlet dew point	90.3 C
Measured inlet dew point	91.3 C
Outlet dew point at OCV	90.2 C

module voltage sweep are listed in Table III. The corresponding voltage / current (VI) or polarization curve is displayed in Figure 19. The average per cell ASR for the initial ILS module, represented by the average slope of the VI curve, was measured to be 2.38 Ωcm^2. This value was significantly higher than the design value of 1.5 Ωcm^2, but was not unexpected. Subcontractor Cermatec Inc, the manufacturer of the ILS module, expected lower performance from this particular module due to manufacturing difficulties they had encountered. After testing samples of cells manufactured since this module, Ceramatec is certain that these problems have been solved and future modules should exhibit higher performance.

Stack internal temperatures initially decreased during the voltage sweep, due to the endothermic heat of reaction for water splitting. Once the operating voltage exceeded the thermal neutral voltage (77V for 60 cells), outlet gas temperatures exceeded inlet values.

Figure 20 presents inlet and outlet dewpoint temperatures and the hydrogen production rate for the ILS initial single-module sweep. The inlet gas dew point remained essentially constant at 89.6°C throughout the duration of the sweep. The

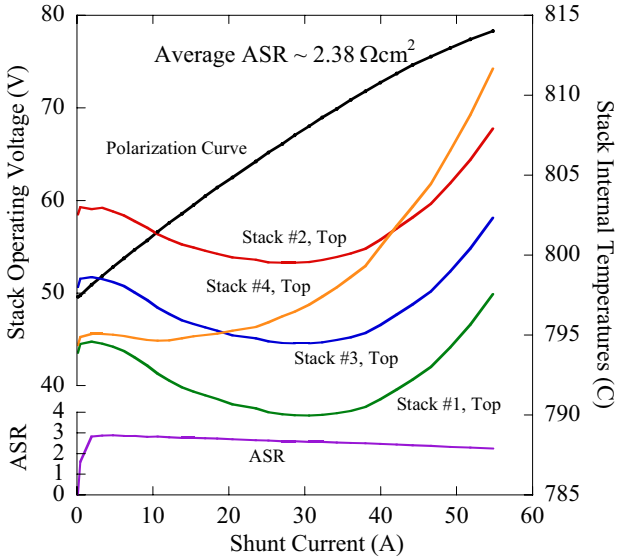

Fig. 19. ILS module voltage sweep / polarization curve.

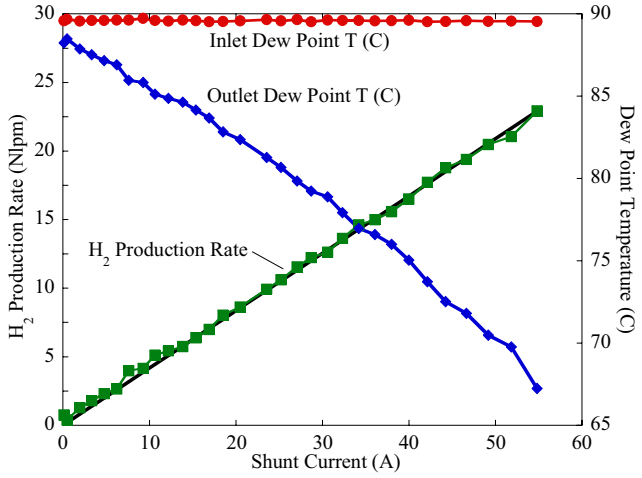

Fig. 20. ILS module voltage sweep hydrogen production rates and dew points.

outlet stream dew point temperature decreased continuously through the sweep as the operating voltage and stack current increased. The straight black line in Figure 20 represents the hydrogen production rate based on electrolysis current, while the green trace is the hydrogen production rate based on the difference between inlet and outlet dew points. Agreement between the two independent measurements of hydrogen production was generally excellent. At the highest current levels, H_2 production rates exceeded 1.4 Nm^3/hr (23 Nlpm).

CONCLUSIONS

The INL, in collaboration with Ceramatec Inc., has been actively researching the use of solid oxide cells for high temperature electrolysis of steam for H_2 production and steam/CO_2 for syngas production. Testing has been conducted at various scales, including button cell (~1 W), stack (~200 W), and the INL ILS facility (5 kW, ultimately 15 kW). Testing has shown high temperature electrolysis to be a promising technology for efficient large-scale production of H_2 and/or syngas.

NOMENCLATURE

ASR	apparent area specific resistance, Ohm cm^2
F	Faraday's constant, 96487 J/V mol
ΔG_f	Gibbs free energy of formation, J/mol
P	pressure, Pa
P_{std}	standard pressure, Pa
R_u	universal gas constant, J/mol K
T	temperature, K
V_N	Nernst potential, V
V_{ref}	reference cell voltage, V
V_{op}	operating voltage, V
y	mole fraction

ACKNOWLEDGMENTS

This work was supported by the U.S. Department of Energy, Office of Nuclear Energy, Nuclear Hydrogen Initiative Program. The Idaho National Laboratory is operated for the U.S. Department of Energy's Office of Nuclear Energy by the Battelle Energy Alliance under contract number DE-AC07-05ID14517.

REFERENCES

[1] Hirsch, R.L., Bezdek, R., Wendling, R., "Peaking of World Oil Production: Impacts, Mitigation, & Risk Management," United States of America Department of Energy NETL Report February, 2005.

[2] Sandalow, D., *Freedom From Oil*, McGraw-Hill, New York, NY, 2008.

[3] O'Brien, J. E., Stoots, C. M., Herring, J. S., and Hartvigsen, J. J.,"Hydrogen Production Performance of a 10-Cell Planar Solid-Oxide Electrolysis Stack," *Journal of Fuel Cell Science and Technology*, Vol. 3, pp. 213-219, May, 2006.

[4] O'Brien, J. E., Stoots, C. M., Herring, J. S., and Hartvigsen, J. J., "High Temperature Electrolysis for Hydrogen Production from Nuclear Energy," invited paper for a NURETH11 Special Edition, *Nuclear Technology*, 2006.

[5] Hawkes, G. L., O'Brien, J. E., Stoots, C. M., Herring, J. S., "CFD Model of a Planar Solid Oxide Electrolysis Cell fro Hydrogen Production from Nuclear Energy," invited paper for a NURETH11 Special Edition, *Nuclear Technology*, 2006.

[6] Herring, J. S., O'Brien, J. E., Stoots, C. M., and Hawkes, G. L., "Progress in High-Temperature Electrolysis for Hydrogen Production using Planar SOFC Technology," *International Journal of Hydrogen Energy*, 2006.

[7] Stoots, C.M., O'Brien, J.E., Hawkes, G.L., Herring, J.S., Hartvigsen, J.J, "High Temperature Co-Electrolysis of H_2O and CO_2 for Syngas Production," *2006 Fuel Cell Seminar*, Honolulu, Hawaii, Nov. 13-17, 2006, paper no. 418.

[8] O'Brien, J. E., Stoots, C. M., Herring, J. S., and Hartvigsen, J. J.,"Hydrogen Production Performance of a 10-Cell Planar Solid-Oxide Electrolysis Stack," *Journal of Fuel Cell Science and Technology*, Vol. 3, pp. 213-219, May, 2006.

[9] Stoots, C. M., O'Brien, J. E., McKellar, M. G., Hawkes, G. L., and Herring, J. S., "Engineering Process Model for High-Temperature Steam Electrolysis System Performance Evaluation," Proc. of the AIChE 2005 Annual Meeting, Cincinnati, Oct. 30 – Nov. 4, 2005.